Research Article

Ultralong Aligned Single-Walled Carbon Nanotubes on Flexible Fluorphlogopite Mica for Strain Sensors

Muhong Wu[1], Kaihui Liu[2], Wenlong Wang[2] (✉), Yu Sui[1] (✉), Xuedong Bai[2] (✉), and Enge Wang[3]

[1] Center for Condensed Matter Science and Technology, Department of Physics, Harbin Institute of Technology, Harbin 150001, China
[2] Beijing National Laboratory for Condensed Matter Physics, Institute of Physics, Chinese Academy of Sciences, Beijing 100190, China
[3] International Center for Quantum Materials, School of Physics, Peking University, Beijing 100871, China

ABSTRACT

Single-walled carbon nanotubes (SWNTs) are expected to be an ideal candidate for making highly efficient strain sensing devices owing to their unique mechanical, electronic, and electromechanical properties. Here we present the use of fluorphlogopite mica (F-mica) as a flexible, high-temperature-bearing and mechanically robust substrate for the direct growth of horizontally aligned ultra-long SWNT arrays by chemical vapor deposition (CVD), which in turn enables the straightforward, facile, and cost-effective fabrication of macro-scale SWNT-array-based strain sensors. Strain sensing tests of the SWNT-array devices demonstrated fairly good strain sensitivity with high ON-state current density.

1. Introduction

Current commercially available strain sensing devices can be generally classified into optical sensors, piezo-electric sensors, and resistance-based sensors. Of these, resistance-based strain sensors are important due to their convenience for a broad range of technological applications [1]. More recently, there has been extensive experimental research on resistance sensors that utilize nanostructured materials as strain-active components [2–5]. However, nanomaterial-based sensing technology is still far away from commercial applications, and the requirements of higher sensitivity, easier fabrication and more cost-effective and cheaper integration are the major challenges in this regard.

Carbon nanotubes, and single-walled carbon nanotubes (SWNTs) in particular, are expected to be an ideal candidate for making highly efficient strain sensing devices owing to their exceptional mechanical, electronic, and especially, unique electromechanical properties. Over the past decade, the electromechanical properties of SWNTs have been well-studied both theoretically [6–8] and experimentally [9, 10]. The electromechanical properties and strain sensing charac-teristics of SWNTs depend on tube chirality. Specifically, quasi-metallic (or small band-gap semiconducting, SGS) SWNTs exhibit the largest sensitivity under axial strain, whilst armchair metallic SWNTs should be the least sensitive to strain response due to their high symmetry (the sub-bands always cross over the Dirac

Springer

point under tensile stretching) [6–10]. As for semi-conducting nanotubes, since semiconducting SWNT devices are normally at the OFF-state at zero gate voltage, it is only when applying a suitable negative gate voltage that the semiconducting SWNTs can exhibit a moderate strain sensitivity with gauge factors larger than armchair metallic SWNTs, but still much less than the SGS SWNTs [9].

The fabrication and operation of nanoscale devices that use individual SWNTs for strain sensing typically needs a sophisticated device design and complex fabrication process, and may suffer from poor reliability due to the variability from sample to sample. As such, there is a need to develop macro-scale strain sensing devices that make use of random SWNT network films or preferably oriented SWNT arrays as conducting channels [2, 3]. Compared with the randomly oriented nanotube networks, the use of horizontally aligned and parallel ultralong SWNT arrays for device fabrication will have significant advantages in terms of manipulation and integration, because they avoid percolation transport pathways, tube/tube junction resistances, and thereby the unusual scaling of device properties [11–22].

Herein, we report on the direct growth of ultralong aligned SWNT arrays by chemical vapor deposition (CVD) on flexible fluorphlogopite mica (F-mica) substrates for strain sensor device fabrication. F-mica is well-known as a layer-structured synthetic crystal that has some superior properties suitable for flexible electronics, such as its high service temperature (up to ~1100 °C), high dielectric constant ($\varepsilon = 5.6$), transparency, wave-penetrativity, anticorrosion, immunity to impurities, infragility, and elasticity. The direct CVD growth of aligned arrays of ultralong SWNTs on F-mica substrates enables the straightforward, facile, and cost-effective fabrication of macro-scale SWNT-array-based strain sensors. Strain sensing tests of the SWNT-array devices demonstrated fairly good strain sensitivity with high ON-state current density. A key advantage of this process is the simplicity and ease of both the fabrication and operation of the sensing devices, in contrast to previously reported sophisticated nanoscale single-tube devices.

2. Experimental

2.1 Synthesis of aligned ultralong SWNTs arrays on F-mica

CVD growth of SWNTs was achieved by employing ordered patterned metal catalyst particles that are derived from self-assembled block copolymer micellar templates [23]. To form micelles with polar poly(4-vinylpyridine) (P4VP) cores in nonpolar polystyrene (PS) domains in toluene solution, 0.4 g of polystyrene–poly(4-vinylpyridine) (PS–P4VP) di-block copolymer was mixed into 100 mL of toluene in a typical experiment, in which 4 mg of anhydrous ferric chloride ($FeCl_3$) was also dissolved in the solution. Fe^{3+} ions stay within the spherical micellar domains due to their interactions with the pyridine units of the PS–P4VP sequester. A monolayer of micelles was formed on F-mica or SiO_2/Si wafers by spin coating of the Fe-loaded polymer micellar solution. Later, one can remove the polymeric shell by applying an O_2 plasma treatment. Both mono-metallic (Fe, Co, Ni, Mo) and bi-metallic (Fe–Mo) particle arrays have been tested in an attempt to control the diameter and even chirality of the aligned ultra-long SWNTs. After O_2 plasma treatment, the wafer with the catalyst will stick on the end of the F-mica substrate. The growth of horizontally aligned ultralong SWNTs on the substrate relies on the CVD method using alcohol as carbon feedstock, a gas flow of 1000/500 standard cubic centimeters per minute (sccm) of H_2/Ar, a growth temperature of 1000 °C and growth time of 30 min.

2.2 Fabrication of the strain sensors and thin-film transistor (TFT) device

Ultraviolet lithography was used to produce the electrode patterns on the samples. 5 nm thick Ti layers and 18 nm thick gold layers were deposited as the electrodes. In order to make the top-gate electrodes, we first made the patterns between source and drain electrodes on the prepared sensor devices using photolithography, then deposited a 10 nm film of Al_2O_3 using atomic layer deposition (ALD) as the top-gate dielectric, and finally deposited 5 nm Ti/18 nm Au

films as the top-gate electrodes, followed by a lift-off process.

2.3 Measurement of strain sensing and transfer characteristics

For testing the strain sensing and transfer characteristics, the prepared sample was located on a precision mechanical stage, and the electrodes of the devices were bonded with gold wires using an ultrasound wire-banded apparatus (Type: F&K5430, from F & K Delvotec Corporation, Germany). The output characteristics, resistance and transfer characteristics of the device were measured using an Agilent series B1500A semiconductor device analyzer, while the sample was bent step by step using the precision mechanical stage. The resistance of the device was measured using the four-probe method.

3. Results and discussion

Figure 1 displays the representative morphology and structure characterization of the as-grown highly aligned ultralong SWNTs arrays on F-mica. Figure 1(a) is an atomic force microscopy (AFM) image of the ordered pattern of the Fe nanoparticle catalyst array, and the inset shows the distribution of the particle diameter. The catalyst nanoparticles were fairly uniform in size. As shown in Figs. 1(b) and 1(c), the spatial distribution of the as-grown nanotubes is very uniform, with tube density around five per hundred microns, facilitating their integration into devices. An AFM image (Fig. 1(c)) reveals that the diameters of the three aligned ultralong carbon nanotubes are 1.181 nm, 1.250 nm and 1.425 nm. Figure 1(d) shows the statistical distribution of the nanotube diameters, ranging from 1 to 2 nm. In this range, the nanotubes should predominantly have a single-walled structure. The diameters of the as-grown nanotubes are uniform and slightly smaller than the initial size of the catalyst nanoparticles. Figure 1(e) displays a typical Raman spectrum of the as-grown SWNT arrays on F-mica substrates. The radial breathing mode (RBM) peak is observed at 193 cm^{-1}, corresponding to the diameter of the SWNT being about 1.24 nm [24]. The sharp G-band peak and
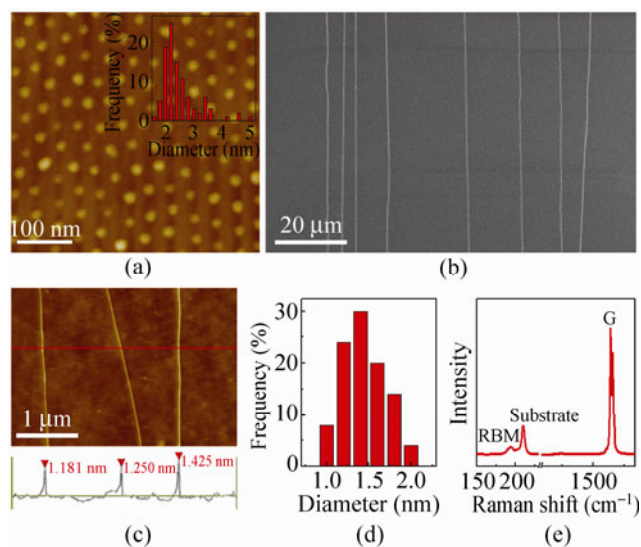
Figure 1 (a) AFM image of the array of iron nanoparticle catalysts; the inset shows the distribution of the size of catalyst particles. (b) SEM image of the aligned ultralong SWNT arrays on F-mica. (c) A typical AFM height image and the corresponding cross-sectional image of SWNT arrays on F-mica. (d) Distribution of the diameters of the nanotubes. (e) Raman spectrum of a SWNT array sample

very low intensity of the D-band peak indicate that the as-grown SWNTs are of high quality.

Figures 2(a)–2(c) show optical images of the aligned ultralong SWNT arrays on a 1 cm × 2 cm F-mica chip. It can be seen that the chip is flexible and transparent after CVD growth. As shown in the scanning electron microscopy (SEM) images in Figs. 2(d)–2(f), the lengths of the as-grown SWNT arrays can be up to ~2 cm, and they grew all over the F-mica substrate. This means that several devices can be fabricated on one substrate through the complementary metal-oxide semiconductor (CMOS)-analogous nanotube-on-insulator (NOI) approach.

A schematic illustration of the fabrication and operation of the strain sensing devices is shown in Fig. 3(a). Figure 3(b) shows a series of output characteristics (I–V curves) while the sensor is bent with a step of 0.5 mm. The inset picture shows the precision mechanical stage used for bending the strain sensor. It can be seen that the current decreases with increasing curvature during the sensor being bent by the stage. As depicted in Fig. 3(c), the normalized resistance change ($\Delta R/R_0$) increases from 0 to 0.27 with strain
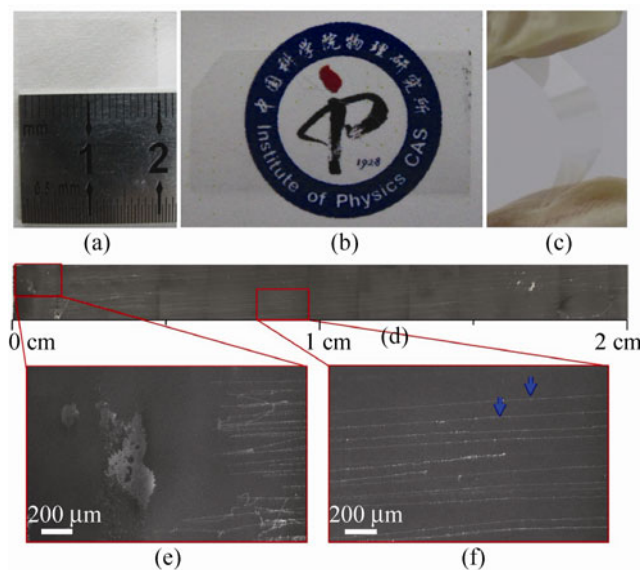
Figure 2 (a), (b) and (c) Optical images of fully transparent flexible aligned ultralong SWNTs arrays on a F-mica chip of size 1 cm × 2 cm. (d) SEM image of the aligned ultralong SWNTs arrays on F-mica. (e) A close-up view of the region covered by the catalyst wafer. (f) A close-up view of the rectangular area with the arrows marking the nanotubes
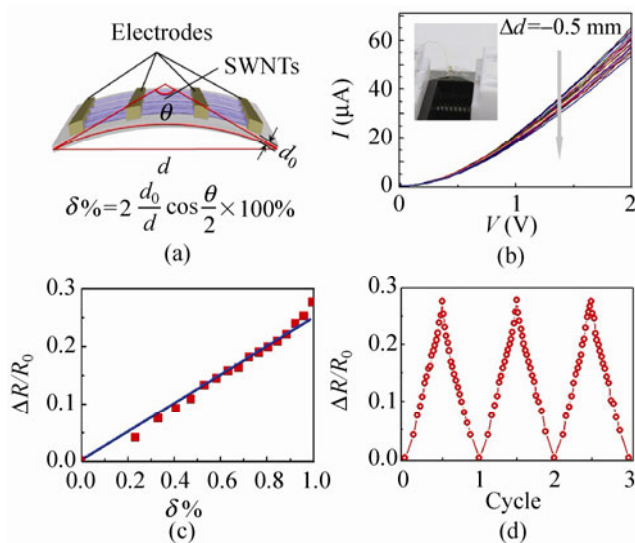
Figure 3 (a) Sketch pattern of the strain sensor based on the aligned ultralong SWNT arrays on F-mica. (b) I–V curves of the sensor with a 0.5 mm step to bending. The inset shows an optical image of the precision mechanical stage with a bent strain sensor. (c) Plot of normalized resistance change vs. strain for the sample. (d) Reversible and reproducible resistance change of the SWNT strain sensor

increasing up to 1%. The relationship between the normalized resistance change and the deformation is approximately linear, as shown by the blue line in

Fig. 3(c). The gauge factor (GF) of the strain sensor can be calculated using the equation:

$$\text{GF} = \frac{\Delta R}{R_0} / \delta \tag{1}$$

where δ denotes the strain induced to gauge, which can be calculated by the equation:

$$\delta\% = 2\frac{d_0}{d}\cos\frac{\theta}{2}\times 100\% \tag{2}$$

where d_0 is the thickness of the substrate, d is the chord length and θ is the bending angle. The relative resistance change is reproducible even after hundreds of repetition cycles (Fig. 3(d)). The corresponding piezoresistance gauge factor is ~27, which is much better than that of conventional strain gauges based on randomly oriented carbon nanotube films, whose reported gauge factors were in the range of 7–10 [2, 3]. Furthermore, the gauge factor is also larger than that for metal alloys [25] and ZnO nanowire paper [26]. However, note that this gauge factor is still an order of magnitude smaller than those of the previously reported single-nanotube devices [9, 10, 27, and 28]. As mentioned above, among the three types of nanotubes, the SGS-SWNTs are the most effective components for strain sensing. Therefore, for either randomly oriented SWNT films or aligned SWNT arrays, the coexistence of the armchair metallic as well as semiconducting nanotubes with the SGS-SWNTs will inevitably compromise the overall sensitivity of the macro-scale strain devices. In addition, since the F-mica substrate used in our work is a layer structured material, the unavoidable problem of layer slippage under bending curvature may also play a role in reducing the strain sensitivity of the devices.

In order to further clarify the working mechanism of the SWNT-array-based sensing devices, we fabricated top-gate field-effect transistor (FET) devices, as schematically illustrated in Fig. 4(a). Figure 4(b) depicts the transfer characteristics (I_{ds}–V_g curves) of the FET device during bending and its recovery process. During bending and recovery, the ON/OFF ratios of the FET devices were ~1.5 and ~1.7 respectively, and the devices could not be depleted completely, with OFF-currents of about 199.4 nA and 169.8 nA, respectively. This

behavior is typical for devices composed of both metallic, SGS and semiconducting SWNTs, as the gate voltage cannot deplete the metallic and SGS SWNTs. Next, we selectively broke down the metallic and SGS nanotubes in the device by using the electrical breakdown method (shown in the inset of Fig. 4(c)), after which the ON/OFF ratios of the device increased to about ~10^4. We then performed comparative measurements of strain-induced resistance changes for the remaining semiconducting SWNTs. As shown in Figs. 4(c) and 4(d), the transfer characteristics when bent and flat were similar, and the strain-induced relative resistance change of the device was minimal. This result clearly indicates that the observed strain sensitivity for the original device shown in Fig. 3 mainly results from the quasi-metallic SGS-SWNTs, plus a small contribution from the armchair metallic SWNTs. Regarding the strain sensing characteristics and band-gap opening mechanism of SGS-SWNTs, a schematic illustration based on the conclusions in the previous literature [6–10] is shown in Fig. 4(e). Unlike the high-symmetry armchair metallic SWNTs whose sub-bands will always cross over the Dirac point under tensile stretching, the SGS-SWNTs are extremely sensitive to axial strain. Since the axial strain will cause deformation of the Brillouin zone, the distance between the sub-band and the Dirac point will increase and thereby induce an increase in band-gap and the resulting resistance. As shown in Refs. [7], and [8], considering the influence of curvature-induced bond length change, the band-gap of some SGS-SWNTs will decrease first and then increase under stretching, corresponding to the variability in change of resistance. This is another reason for the weaker resistance change for the coexisting SGS-SWNTs with different chiralities. As shown in Fig. 4(b), when the resistance change of the SWNT-array device increased to ~27%, the ON/OFF ratio changed slightly from ~1.5 to ~1.7. This result is quite typical of quasi-metallic SGS-SWNT behavior, as the magnitude of strain-induced band-gap opening is only on the order of dozens of meV and cannot surpass the thermal excitation energy at room temperature. Here we note that our result is also in good agreement with the results reported in Ref. [10], where for an individual
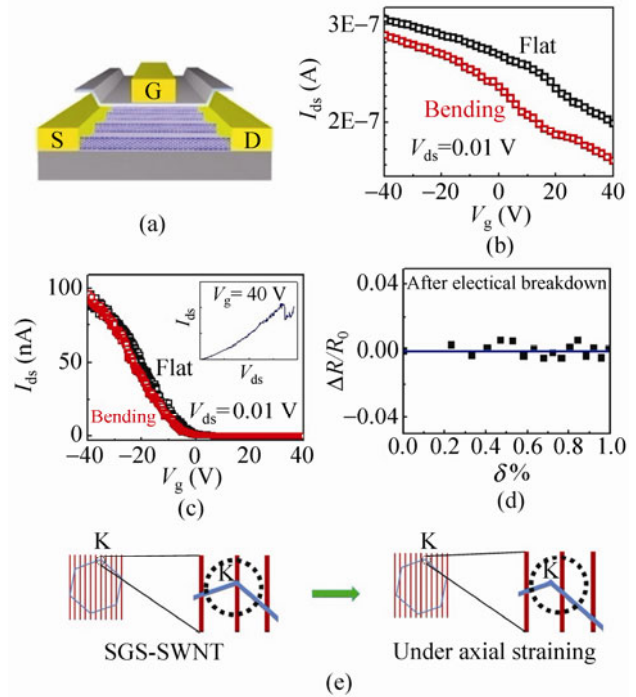
Figure 4 (a) A sketch of the top-gate FET. (b) I_{ds}–V_g curves of the device during bending and flattening. I_{ds}–V_g curves (c) and $\Delta R/R_0$–δ curve (d) of the device during bending and flattening after the metallic SWNTs were removed by electrical breakdown (as shown in the inset of Fig. 4(c)). (e) Schematic illustration of the deformation of the Brillouin zone of SGS-SWNT caused by uniform axial straining. As the tube is strained in the axial direction, the sub-bands (the red lines) will no longer cross the Dirac point (the K point)

SGS-SWNT (Sample 8.1b-CL) under axial strain, the change in ON/OFF ratio was from ~1.8 to ~2.3 when the resistance change was up to ~35%.

4. Conclusions

We have demonstrated a promising route to directly synthesize highly parallel aligned ultralong SWNT arrays on flexible and transparent F-mica substrates. The SWNT arrays on F-mica show the excellent macro-scale sensor characteristics of high sensitivity, high ON-state current density, and easy manipulation and integration. The large-area growth of aligned ultralong SWNT arrays on F-mica substrates is a promising technique for scalable and high-throughput fabrication of nanodevices for flexible and transparent electronics.

Acknowledgements

References

[1] Park, G.; Rosing, T.; Todd, M. D.; Farrar, C. R.; Hodgkiss, W. Energy harvesting for structural health monitoring sensor networks. *ASCE J. Infrastruct. Syst.* **2008**, *14*, 64–79.

[2] Dharap, P.; Li, Z.; Nagarajaiah, S.; Barrera, E. V. Nanotube film based on single-wall carbon nanotubes for strain sensing. *Nanotechnology* **2004**, *15*, 379–382.

[3] Li, Z.; Dharap, P.; Nagarajaiah, S.; Barrera, E. V.; Kim, J. D. Carbon nanotube film sensors. *Adv. Mater.* **2004**, *16*, 640–643.

[4] Lee, Y.; Bae, S.; Jang, H.; Jang, S.; Zhu, S. -E.; Sim, S. H.; Song, Y. I.; Hong, B. H.; Ahn, J. -H. Wafer-scale synthesis and transfer of graphene films. *Nano Lett.* **2010**, *10*, 490–493.

[5] Yu, W. J.; Lee, S. Y.; Chae, S. H.; Perello, D.; Han, G. H.; Yun, M.; Lee, Y. H. Small hysteresis nanocarbon-based integrated circuits on flexible and transparent plastic substrate. *Nano Lett.* **2011**, *11*, 1344–1350.

[6] Nardelli, M. B.; Yakobson, B. I.; Bernholc, J. Mechanism of strain release in carbon nanotubes. *Phys. Rev. B* **1997**, *57*, R4277–R4280.

[7] Yang, L.; Anantram, M. P.; Han, J.; Lu, J. P. Band-gap change of carbon nanotubes: Effect of small uniaxial and torsional strain. *Phys. Rev. B* **1999**, *60*, 13874–13878.

[8] Yang, L.; Han, J. Electronic structure of deformed carbon nanotubes. *Phys. Rev. Lett.* **2000**, *85*, 154–157.

[9] Cao, J.; Wang, Q.; Dai, H. J. Electromechanical properties of metallic, quasimetallic, and semiconducting carbon nanotubes under stretching. *Phys. Rev. Lett.* **2003**, *90*, 157601.

[10] Grow, R. J.; Wang, Q.; Cao, J.; Wang, D. W.; Dai, H. J. Piezoresistance of carbon nanotubes on deformable thin-film membranes. *Appl. Phys. Lett.* **2005**, *86*, 093104.

[11] Huang, S. M.; Cai, X. Y.; Liu, J. Growth of millimeter-long and horizontally aligned single-walled carbon nanotubes on flat substrates. *J. Am. Chem. Soc.* **2003**, *125*, 5636–5637.

[12] Hong, B. H.; Lee, J. Y.; Beetz, T.; Zhu, Y.; Kim, P.; Kim, K. S. Quasi-continuous growth of ultralong carbon nanotube arrays.

J. Am. Chem. Soc. **2005**, *127*, 15336–15337.

[13] Zhou, W. W.; Han, Z. Y.; Wang, J. Y.; Zhang, Y.; Jin, Z.; Sun, X.; Zhang, Y. W.; Yan, C. H.; Li, Y. Copper catalyzing growth of single-walled carbon nanotubes on substrates. *Nano Lett.* **2006**, *6*, 2987–2990.

[14] Reina, A.; Hofmann, M.; Zhu, D.; Kong, J. Growth mechanism of long and horizontally aligned carbon nanotubes by chemical vapor deposition. *J. Phys. Chem. C* **2007**, *111*, 7292–7297.

[15] Ismach, A.; Segev, L.; Wachtel, E.; Joselevich, E. Atomic-step-templated formation of single wall carbon nanotube patterns. *Angew. Chem. Int. Ed.* **2004**, *43*, 6140–6143.

[16] Kocabas, C.; Hur, S. H.; Gaur, A.; Meitl, M. A.; Shim, M.; Rogers, J. A. Guided growth of large-scale, horizontally aligned arrays of single-walled carbon nanotubes and their use in thin-film transistors. *Small* **2005**, *1*, 1110–1116.

[17] Han, S.; Liu, X. L.; Zhou, C. W. Template-free directional growth of single-walled carbon nanotubes on a- and r-plane sapphire. *J. Am. Chem. Soc.* **2005**, *127*, 5294–5295.

[18] Ago, H.; Nakamura, K.; Ikeda, K.; Uehara, N.; Ishigami, N.; Tsuji, M. Aligned growth of isolated single-walled carbon nanotubes programmed by atomic arrangement of substrate surface. *Chem. Phys. Lett.* **2005**, *408*, 433–438.

[19] Louarn, A. L.; Kapche, F.; Bethoux J. M.; Happy, H.; Dambrine, G.; Deryche V.; Chenevier, P.; Izard, N.; Goffman, M. F.; Bourgoin, J. P. Intrinsic current gain cutoff frequency of 30 GHz with carbon nanotube transistors. *Appl. Phys. Lett.* **2007**, *90*, 233108.

[20] Chimot, N.; Derycke, V.; Goffman, M. F.; Bourgoin, J. P.; Happy, H.; Dambrine, G. Gigahertz frequency flexible carbon nanotube transistors. *Appl. Phys. Lett.* **2007**, *91*, 153111.

[21] Ryu, K.; Badmaev, A.; Wang, C.; Lin, A.; Patil, N.; Gomez, L.; Kumar, A.; Mitra, S.; Wong, H. -S. P.; Zhou, C. W. CMOS-analogous wafer-scale nanotube-on-insulator approach for submicrometer devices and integrated circuits using aligned nanotubes. *Nano Lett.* **2009**, *9*, 189–197.

[22] Ishikawa, F. N.; Chang, H. K.; Ryu, K.; Chen, P. C.; Badmaev, A.; De Arco, L. G.; Shen, G. Z.; Zhou, C. W. Transparent electronics based on transfer printed aligned carbon nanotubes on rigid and flexible substrates. *ACS Nano* **2009**, *3*, 73–79.

[23] Bhaviripudi, S.; Reina, A.; Qi, J.; Kong, J.; Belcher, A. M. Block-copolymer assisted synthesis of arrays of metal nanoparticles and their catalytic activities for the growth of SWNTs. *Nanotechnology* **2006**, *17*, 5080–5086.

[24] Jorio, A.; Dresselhaus, G.; Dresselhaus, M. S. Carbon Nanotubes: Advanced Topics in Synthesis, Properties and

Applications; Springer Series in Topics in Apply Physics; Springer-Verlag: Berlin Heidelberg, 2008; Vol. 111.

[25] Chriac, H.; Urse, M.; Rusu, F.; Hison, C.; Neagu, M. Ni–Ag thin films as strain-sensitive materials for piezoresistive sensors. *Sens. Actuator A-Phys.* **1999**, *76*, 376–380.

[26] Gullapalli, H.; Vemuru, V. S. M.; Kumar, A.; Botello-Mendez, A.; Vajtai, R.; Terrones, M.; Nagarajaiah, S.; Ajayan, P. M. Flexible piezoelectric ZnO–paper nanocomposite strain sensor. *Small* **2010**, *6*, 1641–1646.

[27] Stampfer, C.; Helbling, T.; Obergfell, D.; Scho1berle, B.; Tripp, M. K.; Jungen, A.; Roth, S.; Bright, V. M.; Hierold, C. Fabrication of single-walled carbon-nanotube-based pressure sensors. *Nano Lett.* **2006**, *6*, 233–237.

[28] Chang, N. K.; Su, C. C.; Chang S. H. Fabrication of single-walled carbon nanotube flexible strain sensors with high sensitivity. *Appl. Phys. Lett.* **2008**, *92*, 063501.